Available online at www.sciencedirect.com
ScienceDirect
International Journal of Heat and Mass Transfer 50 (2007) 2038–2050
International Journal of HEAT and MASS TRANSFER
www.elsevier.com/locate/ijhmt

Multiplicity analysis of a nonisothermal finite cylindrical catalyst pellet

Gheorghe Juncu *

POLITEHNICA University Bucharest, Catedra Inginerie Chimica, Polizu 1, 78126 Bucharest, Romania

Received 13 July 2006
Available online 28 December 2006

Abstract

The paper examined the steady-state multiplicity behaviour of the porous, non-isothermal, finite cylindrical catalyst pellet in the absence of external transport resistances. A numerical multigrid continuation technique with the preconditioned conjugate gradient squared as coarse grid solver was used. The numerical methods proved to be efficient and reliable so that computations with fine grids (up to 129×129 grid points on the unit square) are easily performed. The key parameter of the investigation is the reaction parameter. The effect of the other governing parameters (especially the aspect ratio) was also analysed. An infinite number of steady states, with a scenario different from that usually used to explain this situation, were obtained at small values of the aspect ratio (the height of the cylinder is greater than the diameter of the cylinder).

Keywords: Finite cylindrical catalyst pellet; Multiplicity; Continuation; Multigrid; Conjugate gradient

1. Introduction

Catalyst particles of cylindrical shape are widely used in industrial processes. In spite of this fact, relatively few published articles analysed the diffusion and reaction phenomena in finite cylinders. The multiplicity and stability of the steady states in a cylindrical catalyst pellet received even less attention.

The diffusion accompanied by an isothermal, first-order irreversible chemical reaction in finite hollow and solid cylinders was investigated in [1–5]. The main goal of these papers was to work-out a relation for the effectiveness factor. An integral equation method was developed in [6,7] to solve the problem of diffusion and reaction in a porous, non-isothermal finite cylindrical pellet in the absence [6]/presence [7] of external transport resistances. Multiplicity features and steady-states stability of a cylindrical catalyst pellet were studied in [8–11].

Sorensen et al. [8] used the orthogonal collocation technique to solve the problem of first-order chemical reaction in a non-isothermal finite cylindrical catalyst pellet with Dirichlet boundary conditions. A predictor–corrector method based on sensitivity analysis was used to obtain the boundaries of the region of multiplicity. Burghardt and Berezowski [9] analysed the multiplicity of the steady states for an infinite cylinder. They found that the parameters domain where multiple steady states exist decreases when the pellet shape changes from the infinite slab to the infinite cylinder to the sphere. The analysis of the stability of the steady state solutions for porous catalytic pellets of different shape can be viewed in [10]. Pan and Zhu [11] draw the conclusion that the multiplicity features for a finite cylinder are analogous to those of an equivalent diameter sphere. The non-isothermal, first-order irreversible chemical reaction in the absence of inter-phase gradients was analysed in [11].

This work wishes to compute the bifurcation diagrams of a finite, non-isothermal, cylindrical catalyst pellet (some results about the finite slab catalyst pellet can be viewed in [12]). This way, we tried to solve two problems: one of

* Tel./fax: +40 21 345 0596.
E-mail addresses: juncu@easynet.ro, juncugh@netscape.net

0017-9310/$ - see front matter © 2006 Elsevier Ltd. All rights reserved.
doi:10.1016/j.ijheatmasstransfer.2006.11.005

Nomenclature

C	concentration of reactant in the pellet
C_B	bulk concentration of the reactant
d	cylinder diameter
D_{eff}	effective diffusivity of reactant in the porous catalyst pellet
E	activation energy of the chemical reaction
H	cylinder height
k_0	pre-exponential factor
r	radial coordinate, cylindrical coordinate system
r^*	dimensionless radial coordinate, 2 r/d, in cylindrical coordinate system
R_G	gas constant
T	temperature of the pellet
T_B	bulk temperature
y	dimensionless concentration of reactant in the pellet, C/C_B
z	axial coordinate, cylindrical coordinate system
z^*	dimensionless axial coordinate, 2 z/H, cylindrical coordinate system

Greek symbols

β	dimensionless adiabatic heat rise (Prater number), $(-\Delta H_R D_{eff} C_B)/(\lambda_{eff} T_B)$
γ	dimensionless activation energy (Arrhenius number), $E/R_G T_B$
ΔH_R	heat of reaction
ε	aspect ratio, d/H
η	effectiveness factor
θ	dimensionless pellet temperature, T/T_B
λ_{eff}	effective thermal conductivity in the porous catalyst pellet
ρ	bulk density of the pellet
ϕ	Thiele modulus, $\varphi = \frac{d}{2}\sqrt{\frac{\rho k_0 \exp(-\gamma)}{D_{eff}}}$

engineering interest (a detailed investigation of the finite cylinder bifurcation behaviour was not made until now) and the other of computational interest (iterative continuation algorithms were tested on a new mathematical model). The chemical reaction is considered first-order irreversible and the inter-phase gradients were neglected. A multigrid (MG) continuation technique was employed to calculate a family of solutions. The coarse grid computations were performed by a preconditioned conjugate gradient algorithm. The path of solutions computed in this work is compared to that provided by the equivalent diameter sphere model [3] (i.e. the sphere that has the ratio volume/external surface equal to that of the cylinder).

2. Mathematical model

Consider a non-isothermal, first-order irreversible chemical reaction taking place inside a finite cylindrical catalyst pellet of diameter d and height H. The inter-phase transport resistances are assumed negligibly. This implies that the concentration and temperature on the external surface of the catalyst pellet are the same as the bulk values. Following the classical formulation presented in [3], which assumes a homogeneous porous pellet and using effective transport coefficients, the steady state concentration and temperature profiles inside the cylinder are given by

$$D_{eff}\Delta C - \rho k_0 C \exp\left(-\frac{E}{R_G T}\right) = 0 \tag{1a}$$

$$\lambda_{eff}\Delta T + (-\Delta H_R)\rho k_0 C \exp\left(-\frac{E}{R_G T}\right) = 0 \tag{1b}$$

where

$$\Delta = \frac{1}{r}\frac{\partial}{\partial r}\left(r\frac{\partial}{\partial r}\right) + \frac{\partial^2}{\partial z^2}$$

with the boundary conditions:

$$-r = 0;$$

$$\frac{\partial C}{\partial r} = \frac{\partial T}{\partial r} = 0 \tag{2a}$$

$$-r = d/2;$$

$$C = C_B, T = T_B \tag{2b}$$

$$-z = 0;$$

$$\frac{\partial C}{\partial z} = \frac{\partial T}{\partial z} = 0 \tag{2c}$$

$$-z = H/2;$$

$$C = C_B, T = T_B. \tag{2d}$$

Defining the dimensionless variables and groups

$$r^* = 2r/d, \quad z^* = 2z/H,$$

$$y = \frac{C}{C_B}, \quad \theta = \frac{T}{T_B}, \quad \varepsilon = \frac{d}{H},$$

$$\beta = \frac{-\Delta H_R D_{eff} C_B}{\lambda_{eff} T_B}, \quad \gamma = \frac{E}{R_G T_B}, \quad \varphi = \frac{d}{2}\sqrt{\frac{\rho k_0 \exp(-\gamma)}{D_{eff}}}$$

the non-dimensional form of (1) is

$$\Delta^* y - \varphi^2 y \exp\left[\gamma\left(1 - \frac{1}{\theta}\right)\right] = 0 \tag{3a}$$

$$\Delta^* \theta + \beta\varphi^2 y \exp\left[\gamma\left(1 - \frac{1}{\theta}\right)\right] = 0 \tag{3b}$$

where

$$\Delta^* = \frac{1}{r^*}\frac{\partial}{\partial r^*}\left(r^*\frac{\partial}{\partial r^*}\right) + \varepsilon^2\frac{\partial^2}{\partial z^{*2}}$$

with the boundary conditions

$$-r^* = 0;$$

$$\frac{\partial y}{\partial r^*} = \frac{\partial \theta}{\partial r^*} = 0 \tag{4a}$$

$$-r^* = 1;$$

$$y = \theta = 1 \tag{4b}$$

$$-z^* = 0;$$

$$\frac{\partial y}{\partial z^*} = \frac{\partial \theta}{\partial z^*} = 0 \tag{4c}$$

$$-z^* = 1;$$

$$y = \theta = 1 \tag{4d}$$

Following the analysis of Prater [13], the system of two partial differential equations (3), can be transformed into a single partial differential equation

$$\Delta^* y - \varphi^2 y \exp\left[\gamma\left(1 - \frac{1}{1+\beta(1-y)}\right)\right] = 0 \tag{5a}$$

and the linear algebraic relation

$$\theta = 1 + \beta(1-y) \tag{5b}$$

relating dimensionless temperature and concentration.

The present results are summarized in terms of:

[-] pellet average dimensionless temperature, $\bar{\theta}$:

$$\bar{\theta} = 2\int_0^1\int_0^1 r^*\theta\,\mathrm{d}r^*\,\mathrm{d}z^* \tag{6a}$$

[-] pellet average dimensionless concentration, $\bar{y}$:

$$\bar{y} = 2\int_0^1\int_0^1 r^* y\,\mathrm{d}r^*\,\mathrm{d}z^* \tag{6b}$$

[-] effectiveness factor, η:

$$\eta = 2\int_0^1\int_0^1 r^* y \exp\left[\gamma\left(1 - \frac{1}{\theta}\right)\right]\mathrm{d}r^*\,\mathrm{d}z^*. \tag{6c}$$

3. Numerical methods

The models equations were discretized with the standard, central second-order accurate, finite difference scheme on grids with $N \times N$ points and steps sizes $h_r = h_z = h = 1/(N-1)$.

Consider that the discrete approximation of the mathematical model equation (5) can be written as

$$G(u,p) = Bu - pg(u) = 0 \tag{7}$$

where $u \in R^n$ corresponds to the field variables, $p \in R$ is the parameter of interest, B an $n \times n$ matrix and g: $R^n \to R^n$ a smooth mapping. For the numerical computation of bifurcation points, two classes of methods can be used: direct methods and indirect methods. In this work, indirect methods were used.

Indirect methods used continuation techniques [14,15], through limit or bifurcation points and distinct methods to accurately locate these points. To pass turning points, the continuation technique necessitates the specification of a new parameter s and an additional equation for s. The reparameterized problem is:

$$G(u,p) = 0 \tag{8a}$$

$$N(u,p,s) = 0 \tag{8b}$$

Equation (8b) is usually named *parametrization equation*. The biggest computational effort of any continuation procedure is the solution of the bordered linear systems

$$\begin{bmatrix} G_u & G_p \\ N_u & N_p \end{bmatrix}\begin{bmatrix} \delta u \\ \delta p \end{bmatrix} = -\begin{bmatrix} G \\ N \end{bmatrix} \tag{9}$$

If G_u is large and sparse (the mathematical model of the process is a 2(3)-D partial differential equation), iterative methods solve usually the system (9) efficiently and accurately.

MG and PGCG methods proved to be the most powerful iterative methods to solve numerically partial differential equations. Nonetheless, these methods have not been used very much in numerical bifurcation techniques. MG and PGCG methods for continuation past bifurcation points are reviewed in [16]. From the software developed until now, the well known and widely used are PLTMG [17] and LOCA [18] (we refer only to software based on iterative methods for 2(3)-D PDE).

PLTMG uses two different parametrization equations, [19,20], and solves the system of nonlinear equations (8) by a combination of a damped Newton iteration and multigraph iteration [21]. The bordered system of equations (9) is solved by a block Gauss elimination procedure. This requires the solutions of two sets of equations using multigraph iteration. LOCA is a library of numerical bifurcation algorithms based on PGCG and bordered methods.

The present continuation technique is a non-bordered iterative algorithm [16], based on the works of Govaerts [22,23]. Let $u^{(0)}$ ($s^{(0)}$), $p^{(0)}$ ($s^{(0)}$) be the solution of (8) and δs the continuation step in s. The elements of the continuation step are:

– Parametrization, [24]

$$N(u,p,s) \equiv \left[\|u - u^{(0)}\|^2 + (p - p^{(0)})^2\right]^{1/2} - \delta s \tag{10}$$

– Predictor step, [24]

$$\bar{u} = u^{(0)} + (\delta s)\frac{u^{(0)} - u^{(-1)}}{(\delta s)^{(0)}} \tag{11a}$$

$$\bar{p} = p^{(0)} + (\delta s)\frac{p^{(0)} - p^{(-1)}}{(\delta s)^{(0)}} \tag{11b}$$

– Corrector step

Newton method applied to (8).

The continuation algorithm acts on a single, coarse grid. The multi-grid cycle used to calculate the fine grid solution is similar to the classical FAS algorithm. The main differences consist of [25]: (a) the parameter p is not altered on fine grids since no high-frequency errors are related to p; on fine grids only equation (7) is smoothed; (b) the coarse grid equation should include the fine grid residuals of all equations; on the coarse grid the enlarged system (8) is solved. The structure of the MG cycle is: (1) cycle of type V; (2) smoothing by point Gauss–Seidel or line Gauss–Seidel (depending on the values of the aspect ratio); two smoothing steps are performed before the coarse grid correction and two after; (3) prolongation by bilinear interpolation for corrections and cubic interpolation for solution; (4) restriction of residuals by full weighting.

The algorithm described previously performs the continuation on a single (coarse) grid. MG methods are used to refine the coarse grid solution. The coarse grid equations (the continuation step and the MG level 1 equations) were solved by the Newton method. The linear solver in a Newton step is the preconditioned conjugate gradient squared (PCGS) algorithm, [26]. The preconditioners used are the incomplete LU factorisation (with two extra diagonals; algorithm IC (1,3) [27]) and the multigrid approximation (two multigrid cycles) of the matrix

$$\begin{bmatrix} B & 0 \\ 0 & 1 \end{bmatrix}.$$

The structure of the MG cycle used in preconditioning is: (1) cycle of type V; (2) smoothing by point or line Gauss-Seidel; one smoothing step is performed before the coarse grid correction and one after in the opposite direction; (3) prolongation by bilinear interpolation; (4) restriction by full weighting; (5) the coarse grid has 5×5 points. The stopping criterion used for PCGS is

$$\frac{\|r_i\|}{\|r_0\|} \leqslant 10^{-6}$$

where r_i is the residual after i iterations and $\|\ \|$ the discrete Euclidean norm. The maximum number of iterations allowed is 1000.

The program starts at low values of p and with a usual continuation algorithm computes some solutions. After a number of steps the program switches to the continuation procedures described previously with δs calculated from the last solutions. The technique for automatically changing the step length δs is presented in [16]. The convergence criterion is:

$$|p^{(k)} - p^{(k-1)}| \leqslant 10^{-5}|p^{(k-1)}| \tag{12}$$

The algorithms described previously gave a method for continuing through bifurcation points. To accurately locate the critical points, the alternative approach, based on Cayley transform and power iteration, was used in this work.

4. Results

The dimensionless mathematical model (5) depends on four non-dimensional parameters: β, γ, ε^2 and ϕ^2. In all simulations, the reaction parameter ϕ^2 was the continuation parameter. Based on the data presented in [3,28,29], β and γ take the values $0 < \beta \leqslant 0.6$, $0 < \gamma \leqslant 28$. Values of the aspect ratio ε between [0.1, 10] cover the situations of practical interest.

This section is divided into two parts. In the first, we analyse the case $\varepsilon = 1$. The second is dedicated to the influence of the aspect ratio on the multiplicity pattern.

4.1. The case $\varepsilon = 1$

The first aspects discussed in this section are of numerical interest. We present results concerning the mesh behaviour of the solutions and the convergence rate of the numerical algorithms.

From the simulations made, we selected for presentation (see Figs. 1–3) those provided by the parameter set, $\beta = 0.4$ and $\gamma = 28.0$. This choice captures the salient numerical problems encountered during the numerical experiments.

Figs. 1–3 show that: (1) the numerical algorithms converge; (2) significant deformation of the bifurcation diagram due to discretization (false bifurcation points, [30]) occurs only on the 5×5 points mesh; (3) the solution stabilizes from the 17×17 points grid; (4) the branches provided by the meshes with $N = 33$, 65, 129 practically overlap (however, the resolution of the graph should be taken into consideration).

For a given parameters set, the convergence rate of PCGS was monitored by the cumulative number of multiplications per grid point and non-linear iteration step. This quantity is an average value calculated for all continuation steps required by a path of solutions on a given mesh. Concerning the convergence rate of PCGS as single grid and coarse grid solver, we can note the following facts (see also Fig. 4):

- the influence of the parameters values on the convergence rate of PCGS is not significant; for example, the differences between a parameters set that exhibits multiplicity and another parameters set that does not exhibit multiplicity are less than 10%;
- the convergence rate is practically the same for all points of the branch;
- CGS, i.e. the non-preconditioned algorithm, converges on all meshes;

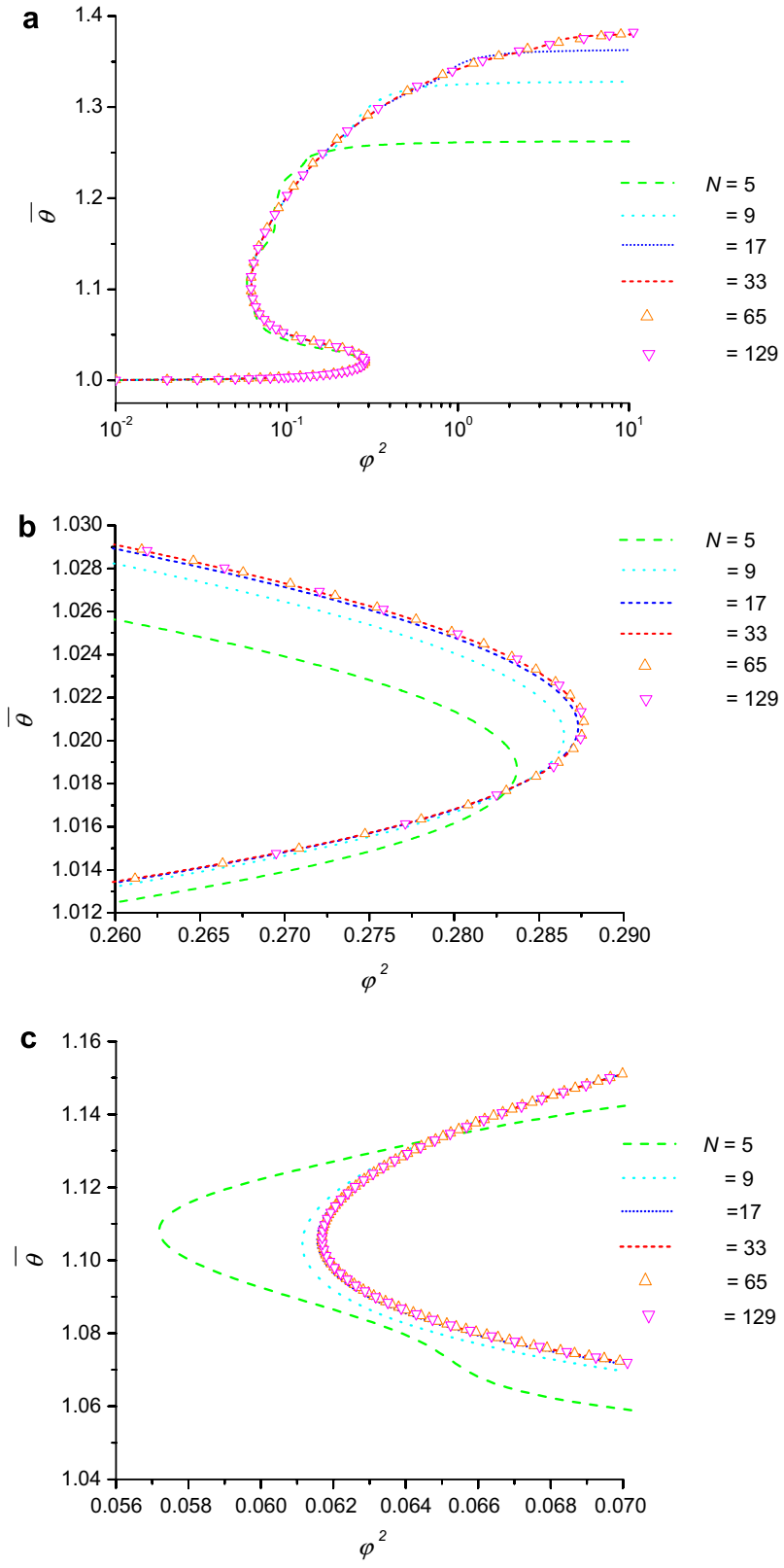

Fig. 1. Solution curves in the $\bar{\theta}$–ϕ^2 diagram; $\beta = 0.4$, $\gamma = 28$ and $\varepsilon = 1$; (a) the entire path of solutions; (b) zoom on the ignition point; (c) zoom on the extinction point.

– preconditioning improves only slightly the robustness and efficiency of the algorithm.

The data plotted in Fig. 4 are average values computed for 20 parameters sets. Restrictions on the continuation

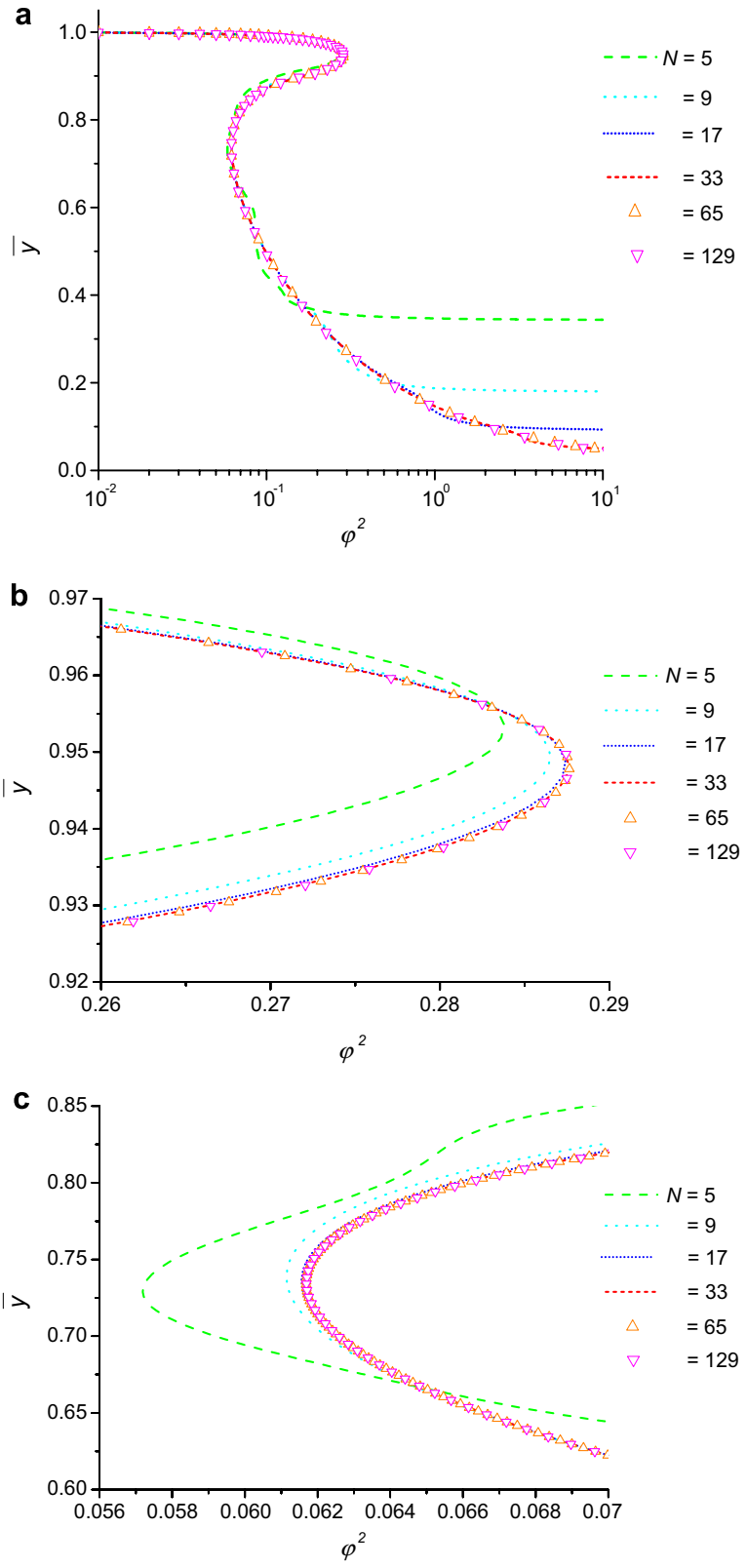

Fig. 2. Solution curves in the $\bar{y}$–ϕ^2 diagram; $\beta = 0.4$, $\gamma = 28$ and $\varepsilon = 1$; (a) the entire path of solutions; (b) zoom on the ignition point; (c) zoom on the extinction point.

step δs were not imposed during the numerical experiments made to evaluate the convergence rate.

Some accidents occurred during the numerical experiments. However, these accidents were isolated and can be

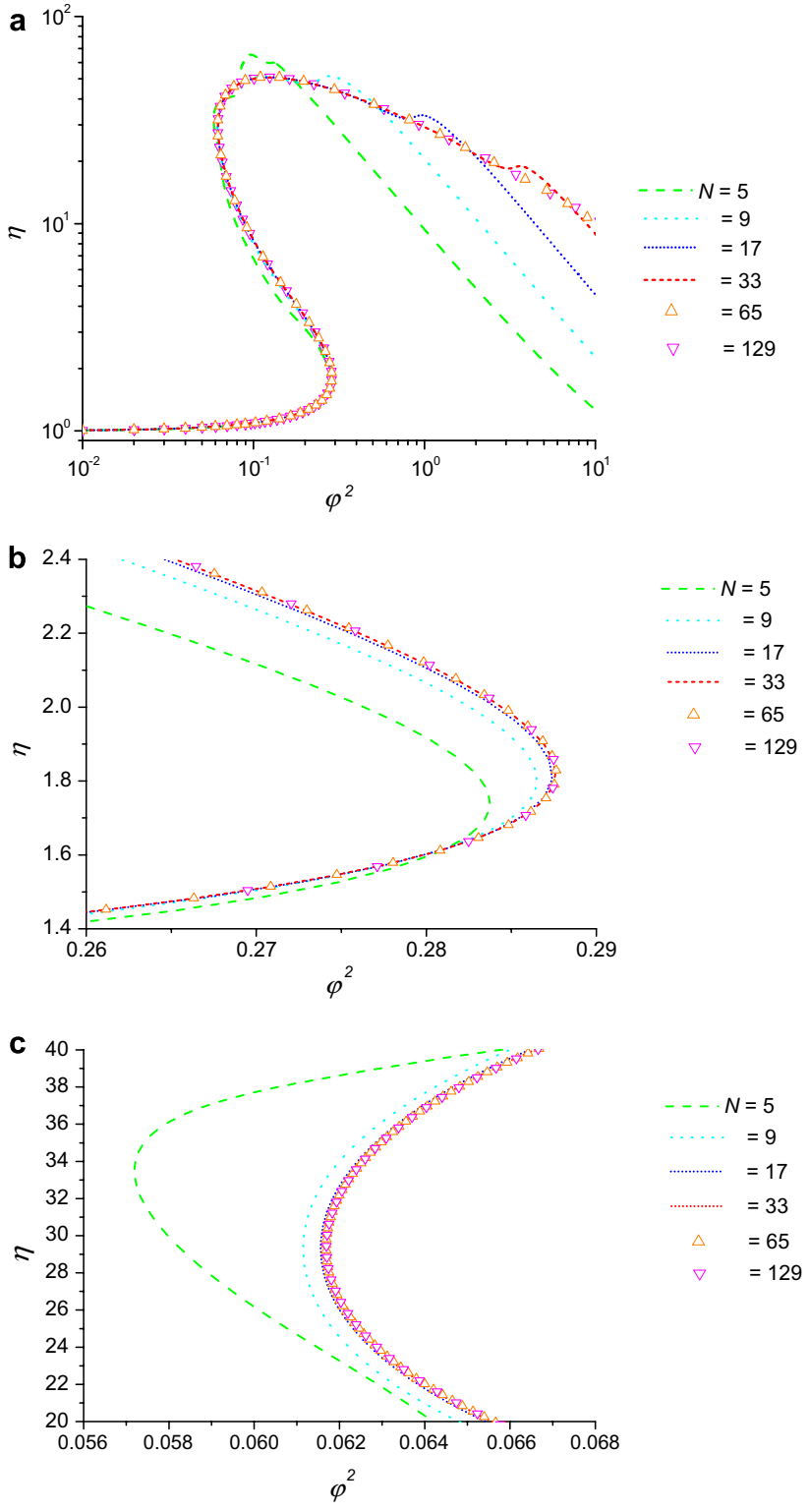

Fig. 3. Solution curves in the η–ϕ^2 diagram; $\beta = 0.4$, $\gamma = 28$ and $\varepsilon = 1$; (a) the entire path of solutions; (b) zoom on the ignition point; (c) zoom on the extinction point.

explained by the typical behaviour of CGS. We cannot state that, for a given parameters set, PCGS as single grid or coarse grid solver fails.

Based on extensive numerical experiments and the results plotted in Figs. 1–3, we selected the following numerical strategy: the continuation is performed on a

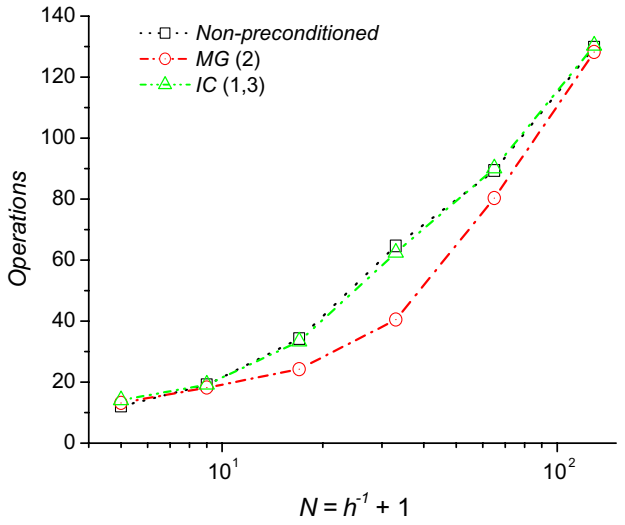

Fig. 4. Mesh behaviour of the convergence rate for PCGS as single grid solver.

mesh having 17×17 points or 33×33 points; the solutions on the grids with $N = 65$ or $N = 129$ is provided by a three level MG algorithm.

The convergence rate of the MG algorithm is given by the average number of MG cycles per continuation step. A value approximately equal to 3, similar to that encountered in usual MG algorithms, was obtained. The solutions obtained on a mesh by MG were always compared to those provided on the same grid by a single grid continuation. Differences between the MG and single grid solutions were not encountered.

Almost all simulations were focussed on the domain $0.4 \leqslant \beta \leqslant 0.6$, $20 \leqslant \gamma \leqslant 28$. In all situations, we obtained only bifurcation diagrams of the type 1–3–1 (only two turning points were detected) similar to those depicted in Figs. 1–3. Some of the turning points calculated are presented in Table 1.

For $\varepsilon = 1$, the mathematical model equations have three parameters. According to [31], the appearance of a swallow-tail point (a singularity of codimension 3) is possible. However, we obtained only bifurcation diagrams corresponding to a non-degenerate hysterezis. A cusp point (a singularity of codimension 2) may be considered as origin of this multiplicity pattern. This behaviour was explained by Meinköhn [32]. The computation of the cusp point and the tracing of the critical boundaries are outside the aims of this work. The computation of the cusp points and of the critical boundaries necessitates specific algorithms, different from the one used here (see [33] and the references cited herein).

Table 1
Numerical values of ϕ^2 at the turning points

γ	β		
	0.4	0.5	0.6
20	0.436967	0.335139	0.272343
	0.2969299	0.145192	0.0743234
24	0.346459	0.268710	0.219642
	0.139077	0.0561847	0.0242189
28	0.287656	0.224502	0.1841895
	0.06169375	0.0204963	0.00742677

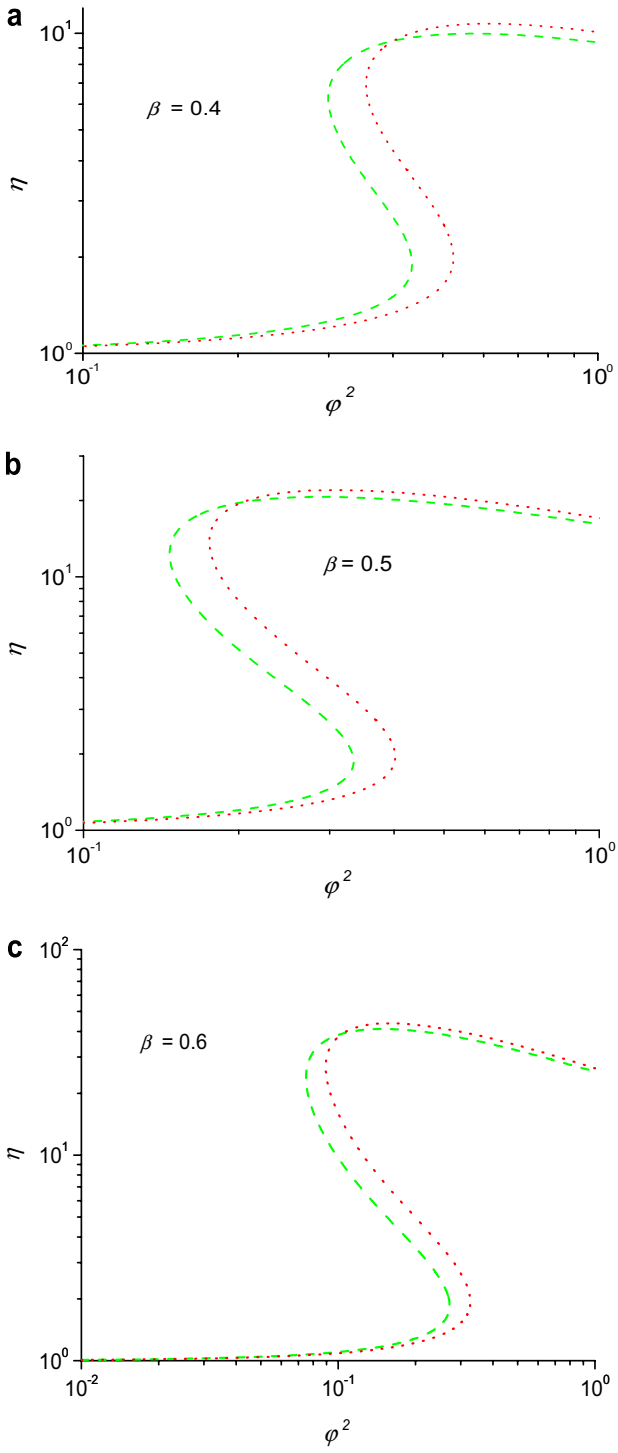

Fig. 5. Comparison between finite cylinder and equivalent sphere response curves; dash lines – finite cylinder results; dot lines – sphere results; $\gamma = 20$ and $\varepsilon = 1$; (a) $\beta = 0.4$; (b) $\beta = 0.5$; (c) $\beta = 0.6$.

The key parameter that expresses the influence of internal diffusion on the chemical reaction rate is the effectiveness factor. In practice, catalyst pellets have different shapes. To calculate the effectiveness factor for each shape is a relatively laborious and inefficient process. To solve this problem, Aris [3] pointed out that a shape independent effectiveness factor is obtained if, in the definition of the Thiele modulus, the ratio (volume)/(surface area) is used as characteristic dimension. Aris's idea became one of the widely used principles in effectiveness factor computation. Based on the same principle, Pan and Zhu [11] established the quasi-equivalence between the critical boundaries of the finite cylinder and the equivalent sphere. Recently, for an isothermal, first-order irreversible chemical reaction, Asif [5] reported deviation up to 12% between the effectiveness factor of the finite cylinder and that of the equivalent sphere.

Fig. 5 shows a comparison between the bifurcation diagrams of the finite cylinder and the equivalent sphere. Note that for $\varepsilon = 1$, the equivalent sphere has the diameter equal to that of the finite cylinder. The results presented in Fig. 5 were obtained on a grid with $N = 129$.

From the data plotted in Fig. 5, we can make the following observations:

- outside the region of turning points, there exists a good agreement between the results of the finite cylinder and the equivalent sphere;
- the bifurcation diagrams have the same shape for both geometries;
- significant quantitative differences occur only in the region of turning points; at the turning points, the absolute value of the relative deviation (cylinder–sphere)/(cylinder) in ϕ^2 is around 20%; this value is practically independent from β.

The situation depicted in Fig. 5 is not characteristic only for the effectiveness factor. The concentration and temperature profiles, expressed by the pellet average values, exhibit the same behaviour with the same maximum deviation.

The same statements would have been made if we had selected a parameters set with constant β and γ variable. We encountered practically this situation in all simulations made at $\varepsilon = 1$, $0.4 \leqslant \beta \leqslant 0.6$ and $20 \leqslant \gamma \leqslant 28$.

4.2. The influence of the aspect ratio on multiplicity pattern

The convergence rate of the numerical algorithms is not influenced significantly by the aspect ratio. We must

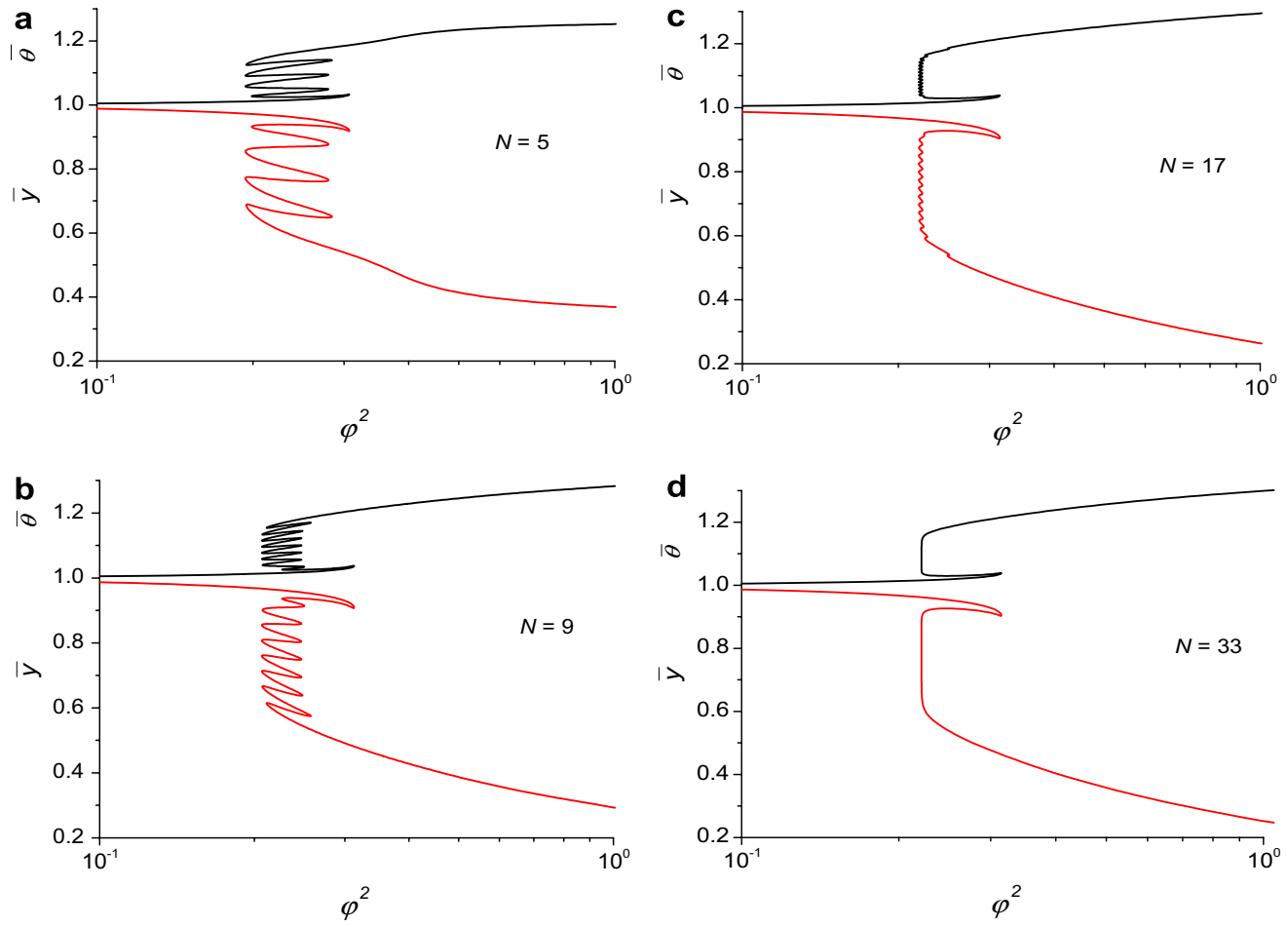

Fig. 6. Mesh behaviour of the solutions for $\beta = 0.4$, $\gamma = 28$ and $\varepsilon = 0.1$; (a) $N = 5$; (b) $N = 9$; (c) $N = 17$; (d) $N = 33$.

mention only one aspect. For $\varepsilon \leqslant 0.2$ or $\varepsilon \geqslant 5$, a severe control of the continuation step δs is necessary. Small values of δs reduce the number of PCGS and MG iterations per continuation step. However, we cannot state that for small or large values of the aspect ratio the convergence rate of the algorithms improves.

The general remarks made in the previous section concerning the influence of discretization on results accuracy remain valid for $\varepsilon \neq 1$. We considered it interesting to present one of the situations encountered at $\varepsilon = 0.1$ (see Fig. 6). Note that for the case plotted in Fig. 6, the branches computed on the grids with $N = 65$ and 129 graphically coincide with that depicted in Fig. 6d ($N = 33$).

The influence of the aspect ratio on the multiplicity pattern is plotted in Fig. 7. The comparison between the cylinder and equivalent sphere results can be viewed in Fig. 8 ($\varepsilon \leqslant 1$) and 9 ($\varepsilon \geqslant 1$). The situation depicted in Figs. 7–9 is not specific only for $\beta = 0.6$ and $\gamma = 20$. It can be considered typical for $0.4 \leqslant \beta \leqslant 0.6$ and $20 \leqslant \gamma \leqslant 28$.

For $\varepsilon < 1$, the most interesting result is the infinite number of steady states obtained at $\varepsilon = 0.1$. Note that the branch computed at $\varepsilon = 0.2$ has only two turning points. Investigating carefully the behaviour of the system for $0.1 \leqslant \varepsilon \leqslant 0.2$, we obtained profiles with an infinite number of steady states for $\varepsilon^2 \leqslant 0.034750$.

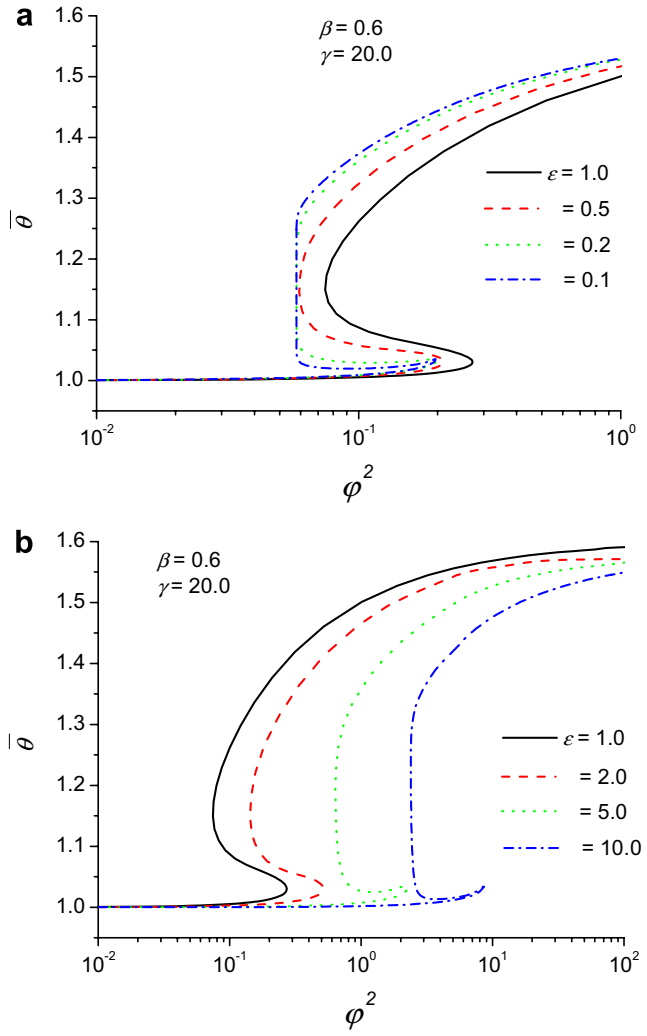

Fig. 7. Bifurcation diagrams for $\beta = 0.6$ and $\gamma = 20$; (a) $\varepsilon \leqslant 1$; (b) $\varepsilon \geqslant 1$.

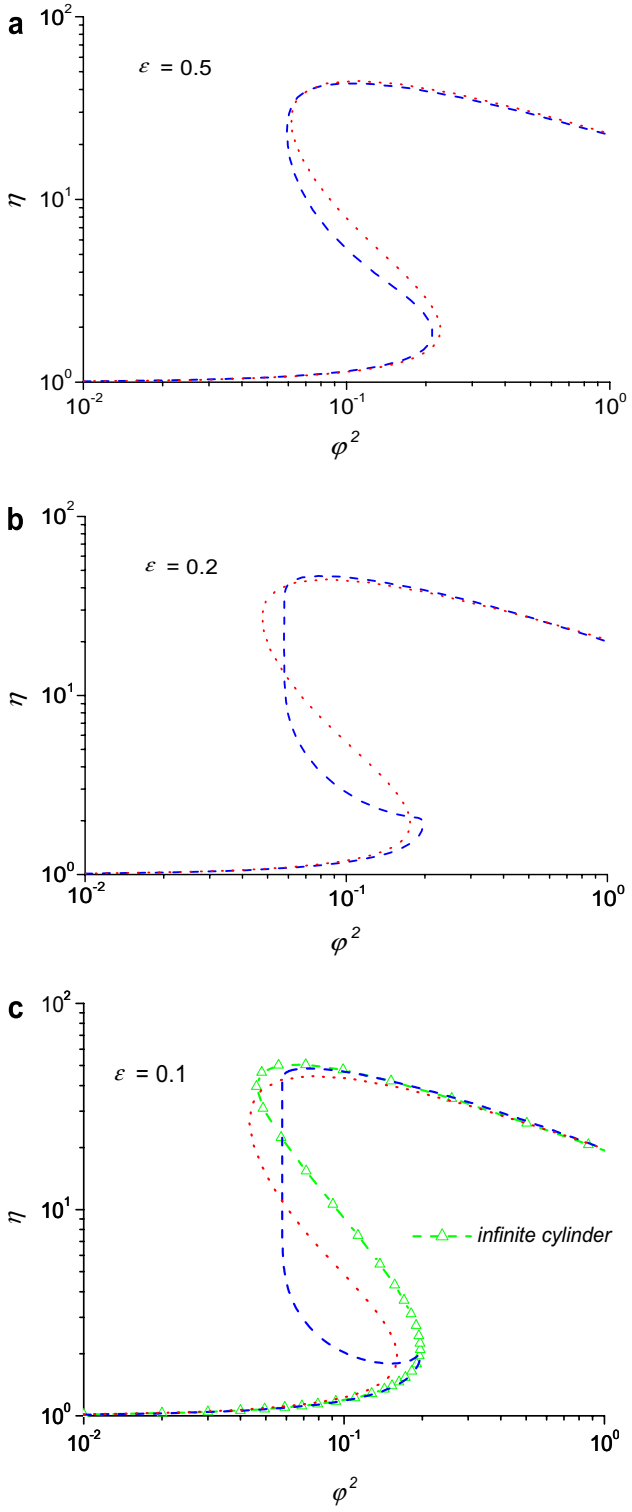

Fig. 8. Comparison between finite cylinder and equivalent sphere response curves; dash lines – finite cylinder results; dot lines – sphere results; $\gamma = 20$ and $\beta = 0.6$; (a) $\varepsilon = 0.5$; (b) $\varepsilon = 0.2$; (c) $\varepsilon = 0.1$.

An infinite number of steady states it is not something new for a catalyst pellet [34–38]. Kapila et al. [35] proved that, in 1 – D, the Dirichlet problem for a non-isothermal first-order Arrhenius kinetics exhibits an infinite number of steady states only in spherical geometry. Witmer et al. [38] considered that an infinite number of steady states is the result of an infinity of imbedded cusps. The scenario proposed by Witmer et al. [38] does not apply to the present situation. The present system does not reach an infinite number of steady states passing through intermediate patterns with 5, 7, ..., steady states. To describe the present situation, we imagine the following mechanical picture: the aspect ratio acts on the bifurcation diagram as someone who pulls a lever in order to put it in vertical position. In [34–38] the infinite number of steady states is the result of the reaction parameters variation, i.e. the parameters that belong to the nonlinear part of the mathematical model (a normal situation because the nonlinear component of the model is responsible for the multiplicity). In our case, the multiplicity pattern changes when a diffusion parameter, i.e. a parameter that occurs in the linear part of the model, changes.

For a given β, the influence of γ variation on the bifurcation diagrams obtained at $\varepsilon = 1$ and $\varepsilon = 0.1$ can be viewed in Fig. 10 (a similar graph is obtained varying β and keeping γ constant). Fig. 10 shows that the bifurcations diagrams calculated for $\varepsilon = 0.1$ have a different shape in comparison with those corresponding to $\varepsilon = 1$. However, in Fig. 10a, only the branches corresponding to $\gamma = 20$ and 28 exhibit an infinite number of steady states.

Concerning the case $\varepsilon < 1$, other noticeable aspects that can be observed in Figs. 7 and 8 are:

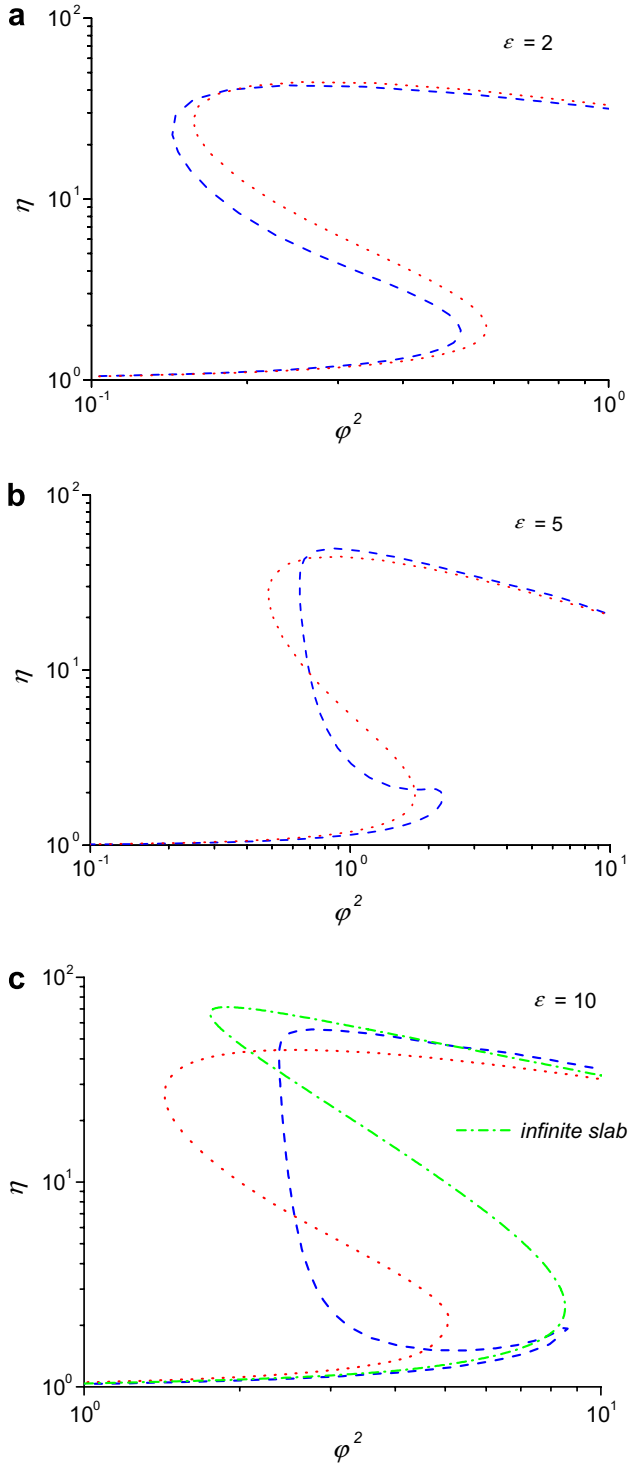

Fig. 9. Comparison between finite cylinder and equivalent sphere response curves; dash lines – finite cylinder results; dot lines – sphere results; $\gamma = 20$ and $\beta = 0.6$; (a) $\varepsilon = 2$; (b) $\varepsilon = 5$; (c) $\varepsilon = 10$.

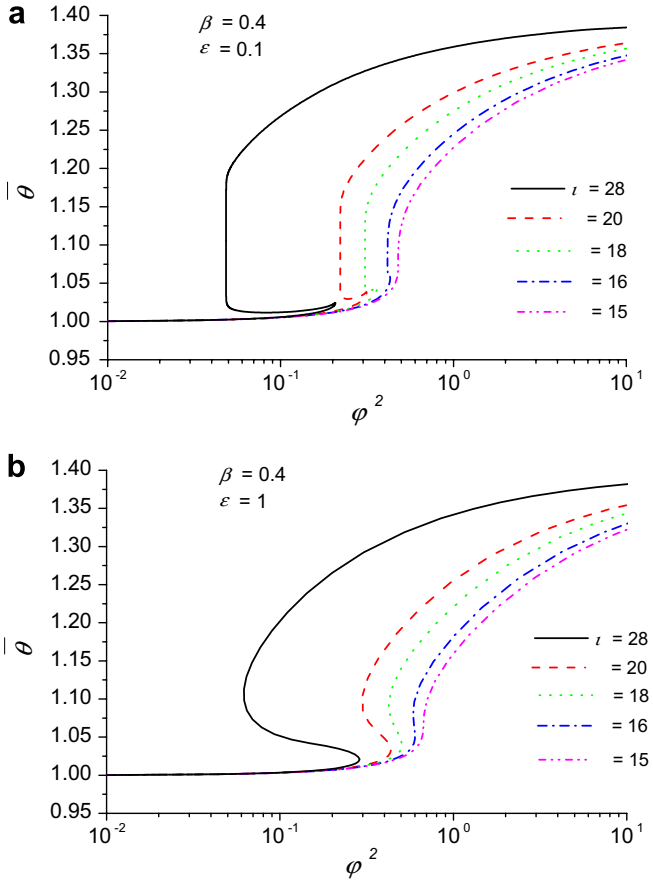

Fig. 10. Bifurcation diagrams for $\beta = 0.4$; (a) $\varepsilon = 0.1$; (b) $\varepsilon = 1$.

– the decrease in the aspect ratio from 0.5 to 0.1 does not change significantly the values of the Thiele modulus at the ignition and extinction points;
– for $\varepsilon = 0.5$ the equivalent sphere model approximates well (even better than at $\varepsilon = 1$) the finite cylinder; the decrease in ε to 0.2 and 0.1 amplifies the differences between the finite cylinder and the equivalent sphere; this behaviour is similar to that presented in [5].

In Fig. 8c, the bifurcation diagram provided by the infinite cylinder is also plotted. The diameter of the infinite cylinder is considered equal to the diameter of the finite cylinder. Fig. 8c shows that the infinite cylinder approximates better than the equivalent sphere the finite cylinder at $\varepsilon = 0.1$. However, the shape of the bifurcation diagram of the infinite cylinder (a typical non-degenerate hysterezis) is different from that of the finite cylinder at $\varepsilon = 0.1$.

For $\varepsilon > 1$, we note the following facts: (1) the increase in ε increases the values of the Thiele modulus at the ignition and extinction points and deforms the shape of the path of solutions; (2) the branches have only two turning points; (3) as in the previous case, the variation in ε has an oscillatory influence on the differences between the finite cylinder and the equivalent sphere; for large values of the aspect ratio, significant differences exist between the two models.

In Fig. 9c, the bifurcation diagram provided by the infinite slab is also plotted. The characteristic dimension of the infinite slab is $H/2$. Note that for the infinite slab, the present results are in excellent agreement with those presented in [33,39,40]. Fig. 9c shows that the infinite slab approximates better than the equivalent sphere the finite cylinder at $\varepsilon = 10$. However, we cannot state that a good agreement exists between the bifurcation diagrams of the infinite slab and the finite cylinder.

5. Conclusions

The bifurcation diagrams of a non-isothermal finite cylinder catalyst pellet were calculated neglecting the external gradients. A numerical MG continuation technique with psedo-arc-length parametrization was applied to the finite difference approximation of the mathematical model. The bifurcation diagrams computed for the finite cylinder are compared to those provided by the equivalent sphere model.

The influence of the aspect ratio on the multiplicity pattern is the most important result obtained in this work. For $\varepsilon = 1$, the behaviour of the system is the typical one for a catalytic diffusion-reaction systems in the absence of external resistances. Bifurcation diagrams generated by a cusp singularity were obtained. For small values of the aspect ratio, concretely at $\varepsilon = 0.1$, a multiplicity pattern with an infinite number of steady states occurs. The path from the usual non-degenerate hysterezis to an infinite number of steady states is different from that encountered in other situations.

References

[1] D.J. Gunn, Diffusion and chemical reaction in catalyst and absorption, Chem. Eng. Sci. 22 (11) (1967) 1439–1455.
[2] D. Luss, N.R. Amundson, On a conjecture of Aris: proof and remarks, A.I.Ch.E.J. 13 (4) (1967) 759–763.
[3] R. Aris, The Mathematical Theory of Diffusion and Reaction in Permeable Catalysts, Calendron Press, Oxford, 1975.
[4] T.C. Ho, G.C. Hsiao, Estimation of the effectiveness factor for a cylindrical catalyst support: a singular perturbation approach, Chem. Eng. Sci. 32 (1) (1977) 63–66.
[5] M. Asif, Efficient expressions for effectiveness factor for a finite cylinder, Chem. Eng. Res. Design 82 (A5) (2004) 605–610.
[6] S. Mukkavilli, L.T. Tavlarides, C.W. Wittmann, Integral method of analysis for chemical reaction in a nonisothermal finite cylindrical catalyst pellet – I. Dirichlet problem, Chem. Eng. Sci. 42 (1) (1987) 27–33.
[7] S. Mukkavilli, L.T. Tavlarides, C.W. Wittmann, Integral method of analysis for chemical reaction in a nonisothermal finite cylindrical catalyst pellet – II. Robin problem, Chem. Eng. Sci. 42 (1) (1987) 35–40.
[8] J.P. Sorensen, E.W. Guertin, W.E. Stewart, Computational models for cylindrical catalyst particles, A.I.Ch.E.J. 19 (1973) 969–975.
[9] A. Burghardt, M. Berezowski, Analysis of the structure of steady-state solutions in a porous catalyst pellet. Part 1: determination of parameter regions with different bifurcation diagram, Chem. Eng. Process 26 (1) (1989) 43–57.
[10] A. Burghardt, M. Berezowski, Stability analysis of steady-state solutions for porous catalytic pellets: influence of the shape of the pellet, Chem. Eng. Sci. 50 (4) (1995) 661–671.
[11] T. Pan, B. Zhu, Study on diffusion – reaction process inside a cylindrical catalyst pellet, Chem. Eng. Sci. 53 (5) (1998) 933–946.
[12] Gh. Juncu, Multiplicity analysis of a nonisothermal finite slab catalyst pellet, Rev. Chimie 56 (11) (2005) 1085–1089.
[13] C.D. Prater, The temperature produced by heat of reaction in the interior of porous particles, Chem. Eng. Sci. 8 (3/4) (1958) 284–286.
[14] R. Seydel, V. Hlavacek, Role of continuation in engineering analysis, Chem. Engng. Sci. 42 (1987) 1281–1295.
[15] E.L. Allgower, K. Georg, Numerical path following, in: P.G. Ciarlet, J.L. Lions (Eds.), Handbook of Numerical Analysis, vol. 5, North-Holland, Amsterdam, 1997, available on line from http://www.math.colostate.edu/emeriti/georg/georg.publications.html.
[16] Gh. Juncu, E. Mosekilde, C. Popa, Numerical experiments with MG continuation algorithms, Appl. Num. Math. 56 (2006) 844–861.
[17] R.E. Bank, PLTMG: A software package for solving elliptic partial differential equations. Users' Guide 9.0. Dept. of Math. University of California at San Diego: La Jola, USA, 2004. available on line from http://www.scicomp.ucsd.edu/~reb/.
[18] A.G. Salinger, N.M. Bou-Rabee, E.A. Burroughs, R.B. Lehoucq, R.P. Pawlowski, L.A. Romero, E.D. Wilkes, LOCA 1.1: Library of Continuation Algorithms, Theory and Implementation Manual. Sandia National Laboratories: Albuquerque, USA, 2002. available on line from http://www.cs.sandia.gov/LOCA.
[19] H.D. Mittelmann, H. Weber, Multi-grid solution of bifurcation problems, SIAM J. Sci. Statist. Comput. 6 (1985) 49–60.
[20] R.E. Bank, T.F. Chan, PLTMG: A multigrid continuation program for parameterized nonlinear elliptic systems, SIAM J. Sci. Stat. Comput. 7 (1986) 540–559.
[21] R.E. Bank, R.K. Smith, An algebraic multilevel multigraph algorithm, SIAM J. Sci. Comput. 23 (5) (2002) 1572–1592.
[22] W. Govaerts, Stable solvers and block elimination for bordered systems, SIAM J. Matrix Anal. Appl. 12 (3) (1991) 469–483.
[23] W. Govaerts, Solution of bordered singular systems in numerical continuation and bifurcation, J. Comput. Appl. Math. 50 (1994) 339–347.
[24] N. Dinar, H.B. Keller, Computations of Taylor vortex flows using multigrid continuation methods, Lecture Notes in Engineering 43, Springer, Berlin, 1989, 191–262.

[25] W. Hackbusch, Multi-grid solution of continuation problems, Lecture Notes in Mathematics, 953, Springer, Berlin, 1982, 20–43.
[26] P. Sonneveld, CGS, A fast Lanczos – type solver for nonsymmetric linear systems, SIAM J. Sci. Statist. Comput. 10 (1) (1989) 36–52.
[27] J.A. Meijerink, H.A. van der Vorst, Guideliness for the usage of incomplete decompositions in solving sets of linear equations as they occur in practical problems, J. Comput. Phys. 44 (1981) 134–155.
[28] L.K. Doraiswamy, M. Sharma, Heterogeneous Reactions: Analysis, Examples and Reactor Design, Wiley, New York, 1984.
[29] G.F. Froment, K.B. Bischoff, Chemical Reactor Analysis and Design, Wiley, New York, 1990.
[30] J. Bigge, E. Bohl, Deformations of the bifurcation diagram due to discretization, Math. Comput. 45 (172) (1985) 393–403.
[31] M. Golubitski, D.G. Schäffer, Singularities and Groups in Bifurcation Theory I, Springer, Berlin, 1985.
[32] D. Meinköhn, Singularity theory concepts for a class of reaction – diffusion systems, Chem. Engng. Sci. 46 (1) (1991) 265–272.
[33] Gh. Juncu, S. Bildea, Bifurcation points computation of the diffusion – reaction equations, Computers Chem. Engng. 16 (12) (1992) 1059–1062.
[34] J.M. Vega, A. Linan, Isothermal *n*th order reaction in catalytic pellets. Effect of external mass transfer resistance, Chem. Eng. Sci. 34 (11) (1979) 1319–1322.
[35] A.K. Kapila, B.J. Matkowsky, J.M. Vega, Reactive – diffusive system with Arrhenius kinetics: peculiarities of the spherical geometry, SIAM J. Appl. Math. 38 (3) (1980) 382–491.
[36] J.M. Vega, A. Linan, Singular Langmuir–Hinshelwood reaction – diffusion problems: strong solution under quasi-isothermal condition, SIAM J. Appl. Math. 42 (5) (1982) 1047–1068.
[37] J.M. Vega, Singular Langmuir–Hinshelwood reaction – diffusion problems: strongly nonisothermal conditions, SIAM J. Appl. Math. 43 (6) (1983) 1357–1389.
[38] G.S. Witmer, W. Balakotaiah, D. Luss, Multiplicity features of distributed systems -1. Langmuir–Hinshelwood reaction in a porous catalyst, Chem. Eng. Sci. 41 (1) (1986) 179–186.
[39] R. Seydel, Numerical computation of branch points in ordinary differential equations, Numer. Math. 32 (1979) 51–68.
[40] G. Moore, A. Spence, The calculation of turning points of nonlinear equations, SIAM J. Numer. Anal. 17 (4) (1980) 567–576.